Manganese double substituted pyrochlore type semiconducting oxides for high temperature NTC thermistor applications

S. Sumi · P. Prabhakar Rao · Peter Koshy

Abstract The effect of simultaneous substitution of Mn in both A and B sites of the pyrochlore type semiconducting oxides: $(CaCe_{1-2x}Mn_{2x})(Sn_{1-x}Mn_xNb)O_{7-\delta}$ ($x = 0$, 0.1, 0.2, 0.3 and 0.4) was studied by employing powder X-ray diffraction, Raman spectroscopy, scanning electron microscopy and electrical conductivity measurements. Besides the structural confirmation, Raman spectroscopy studies revealed the increased local disordering in the structure with progressive Mn substitution which is not observable in X-ray diffraction studies. The conductivity measurements confirm the negative temperature coefficient (NTC) behavior of the samples. Grain boundary dominant electrical characteristics have been observed in compounds with higher Mn concentration. Thermistor constant of the system lies in the range 6,700–8,500 K and the sensitivity values are in the range −1 to −2 %. The double substitution of Mn in this system offers to tune the NTC thermistor properties with increased localization of electrons in the lattice.

1 Introduction

Pyrochlore structure have the general formula $A_2B_2O(1)_6O(2)$, A and B being distinct sites to be occupied by cations of several valences. It is a highly chemically and thermally stable structure which can accommodate wide variety of chemical substitutions and structural defects. This unique nature of pyrochlore structure gifted the materials scientists with numerous materials of interest with rich crystal chemistry and interesting transport properties such as superconductivity [1], semiconductivity [2], magnetism [3], luminescence properties [4], etc. The structure can be viewed as an interpenetrating networks of BO_6 octahedra and $A_2O(2)$ chains. Manganese containing pyrochlores are always a point of attraction due to its fascinating electrical and magnetic properties [5, 6]. The mixed valence nature of manganese can be effectively utilized in the formation of new pyrochlores as it can take different crystallographic positions of pyrochlore. Mn^{2+} [VIII; r (Å) = 0.96] would prefer to occupy at the A site and Mn^{3+} [VI; r (Å) = 0.645] and Mn^{4+} [VI; r (Å) = 0.53] prefer to occupy the B site based on the coordination requirement [7].

There is an ever increasing demand for precise temperature measurement and control in line with the advancement of modern technology. Temperature sensors are essential not only in domestic and industrial activities but also in laboratory and medical applications. Currently temperature sensors based on negative temperature coefficient of resistance (NTCR) ceramic thermistors are mainly spinel structured compounds containing transition metals like Ni, Mn, Cu, and Fe [8]. But many of them lack phase purity, density, thermal stability, etc. Also their applications are limited to temperatures below 300 °C due to their instability and changing electrical characteristics at high temperatures. Despite of high tolerance, thermal and chemical stability pyrochlore structured NTC thermistors are rarely reported [5, 9]. It is also reported that the thermistor properties can be effectively tuned with suitable chemical substitutions [10]. Our earlier work on substituting Mn in Ce site of the $CaCeSnNbO_7$ pyrochlore structured semiconducting oxide revealed the effect of Mn substitution on the electrical properties of the materials and

S. Sumi · P. Prabhakar Rao (✉) · P. Koshy
Materials Science and Technology Division, National Institute for Interdisciplinary Science and Technology (NIIST), Thiruvananthapuram 695 019, India
e-mail: padala_rao@yahoo.com

observed that localization of electrons associated with Mn^{2+} played an important role in the tuning of electrical properties and hence the NTC thermistor behavior of the compounds [5]. It was found that the thermistor properties can be improved by increasing the amount of Mn^{2+} in the A site of the pyrochlore. Though Mn predominantly existed as Mn^{2+}, for higher Mn concentration the presence of Mn^{4+} has been identified and it prefers to occupy at the B site by successfully replacing Sn from its site. Thus higher substitution of Mn at A site led to secondary phase formation. It is expected that double substitution of Mn at A and B sites would allow increasing the amount of substitution and hence enhancing the control of transport properties.

Impedance spectroscopy can be successfully employed as a powerful tool to understand the contribution of different RC elements to the NTC behavior of materials. These understandings motivated us to prepare compounds in which more Mn ions could exist in the Ce site as Mn^{2+} and comparably less amount of Mn in the Sn site as Mn^{4+}. In the present investigation, we have explored the possibility of simultaneous substitution of Mn in both A (Ce site) and B (Sn) site of the pyrochlore thereby improve the NTC thermistor properties of the materials.

2 Experimental

Polycrystalline samples of $CaCe_{1-2x}Mn_{2x}Sn_{1-x}Mn_x$ $NbO_{7-\delta}$ ($x = 0$, 0.1, 0.2, 0.3 and 0.4) were synthesized through the conventional solid-state route using the starting materials $CaCO_3$ (99.9 %, Acros Organics), CeO_2 (99.9 %, Aldrich), MnO_2 (99.5 %, Merck), SnO_2 (99.9 %, Aldrich), and Nb_2O_5 (99.5 %, Aldrich). The constituent chemicals taken in stoichiometric ratios, were mixed thoroughly in an agate mortar with acetone as the mixing aid. The mixture was then dried by keeping in a hot air oven at 100 °C. The process of mixing and drying was repeated thrice to get a homogeneous mixture. The powdered samples were calcined at 1,200 °C for 6 h. The calcined powder was then made into pellets with 10 mm diameter and 2 mm thickness by isostatic pressing at a pressure of 250 MPa. 4 wt% polyvinyl alcohol (PVA) was added as a binder for good compaction of the pellets. The pellets were heated at 600 °C for 1 h to burn off the PVA and then sintered at 1,250 °C for 9 h.

Powder X-ray diffraction technique was employed to identify the crystal structure of the compounds using a Ni filtered Cu Kα radiation using a PANalytical X'pert Pro diffractometer. Raman spectra were recorded using a HR800 LabRAM confocal Raman spectrometer operating at 20 mW laser power equipped with a peltier cooled CCD detector. Samples were excited using a He–Ne laser source

having an excitation wavelength of 632.8 nm and with an acquisition time of 5 s using a 50× microscope objective. All the spectra are presented after baseline correction. The microstructure of the samples was recorded by a scanning electron microscope (SEM) of JEOL JSM 5600 on the thermally etched polished pellets. The dc conductivity of the pellet was recorded from 30 to 600 °C using a 6½ digit digital multimeter. For that the pellets were coated with a high temperature silver paste and cured at 600 °C for 30 min and silver wires were attached to the silver coated surfaces. The ac impedance analysis of the samples was carried out by a computer-controlled impedance analyzer (Solartron, SI 1260) in the frequency range 10 Hz to 1 MHz. The complex impedance plots were made with SMART software supplied by M/s Solartron.

3 Results and discussion

3.1 X-ray diffraction studies

Powder X-ray diffraction patterns of the compositions: $(CaCe_{1-2x}Mn_{2x})(Sn_{1-x}Mn_xNb)O_{7-\delta}$ ($x = 0$, 0.1, 0.2, 0.3 and 0.4) are shown in Fig. 1. In our earlier studies, 40 mol% of Mn was able to accommodate at the A site as Mn^{2+} and afterwards Mn shows a tendency to form Mn^{4+} and replaced Sn from the B site thereby produced SnO_2 secondary phases. In the present investigation, substitution of cerium with Mn yielded a complete solid solution in the range $0.1 \leq x \leq 0.3$. i.e., about 60 mol% of Mn could able to accommodate at the A site as Mn^{2+}. Afterwards, minor peaks of MnO_2 can be seen. The splitting of the diffraction peaks can be observed for $x = 0$ which is a clear indication
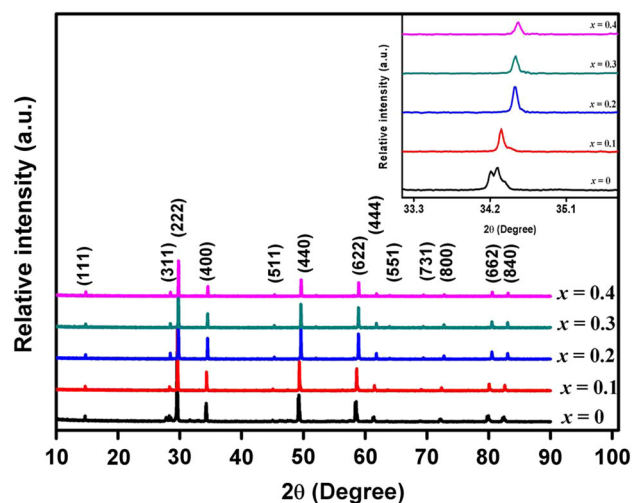

Fig. 1 Powder XRD patterns of $(CaCe_{1-2x}Mn_{2x})(Sn_{1-x}Mn_xNb)O_{7-\delta}$ ($x = 0$, 0.1, 0.2, 0.3 and 0.4) samples. The shift in diffraction peak at around 34° 2θ with increase in x is shown in the *inset*

of the lowering of symmetry from the cubic pyrochlore. The shift in diffraction peaks towards higher angle region with increase in x (inset of Fig. 1) is directly related to the lowering in average ionic radius of Ce^{3+} (1.143 Å), Mn^{2+} (0.96 Å), Sn^{4+} (0.69 Å) and Mn^{4+} (0.53 Å). This observation is also an indication of incorporation of Mn in Ce site as well as in Sn site. An increase in structural ordering was able to observe in the earlier case but no such structural ordering is observable in the present investigation with simultaneous substitution of Mn from the X-ray diffraction studies.

3.2 Raman analysis

Raman spectroscopy is a very sensitive tool to metal-oxygen vibrational modes and reveals the details of local disordering in compounds. It is used as a probe to follow the changes in the anion sublattice with substitution and hence becomes an important complement to X-ray diffraction. Factor group analysis on cubic pyrochlores, $A_2B_2O(1)_6O(2)$, belong to the space group Fd-3 m (No. 227), where $Z = 8$ with the following site symmetries predicted six Raman-active modes. The corresponding factor group for the cubic pyrochlore is O_h and the site symmetry is D_{3d} for the A and B cations, C_{2v} for the O(1) anion, and T_d for the O(2) anion. The irreducible representations of the six Raman-active modes are given as follows [11, 12];

$$\Gamma(\text{Raman}) = A_{1g} + E_g + 4F_{2g} \qquad (1)$$

Figure 2 shows the FT Raman spectra of sintered $CaCe_{1-2x}Mn_{2x}Sn_{1-x}Mn_xNbO_{7-\delta}$ ($x = 0, 0.1, 0.2$ and 0.3) samples taken at room temperature. All the Raman modes involve the motion of oxygen atoms. The modes present in the compounds confirm the cubic pyrochlore structure. Among the six Raman active modes five modes can be clearly seen in the spectra. The A_{1g} mode is present at ~ 510 cm^{-1}, E_g at ~ 350 cm^{-1} and the F_{2g} modes are at $\sim 280, 400, 580$ and 750 cm^{-1} [13]. The displacement of oxygen atoms on both 48f and 8b sites are involved in the F_{2g} modes while the A_{1g} and E_g modes are associated with the movements of 48f oxygen only. The only vibrational mode associated with the A–O interaction is the F_{2g} mode at ~ 280 cm^{-1}. It is found to be broad for the Mn substituted samples. This broadening can be correlated with the oxygen vacancies present in the system as we substitute Mn^{2+} in place of Ce^{3+} [14]. The E_g mode was found to be merged with the F_{2g} mode ~ 400 cm^{-1} and hence found to be broad. With progressive substitution of Mn in both A and B sites, A_{1g} became the most prominent mode of vibration. A_{1g} mode is associated with B–O bending vibrations. In pyrochlores, the rigidity of the structure depends on the BO_6 octahedral network. It has been
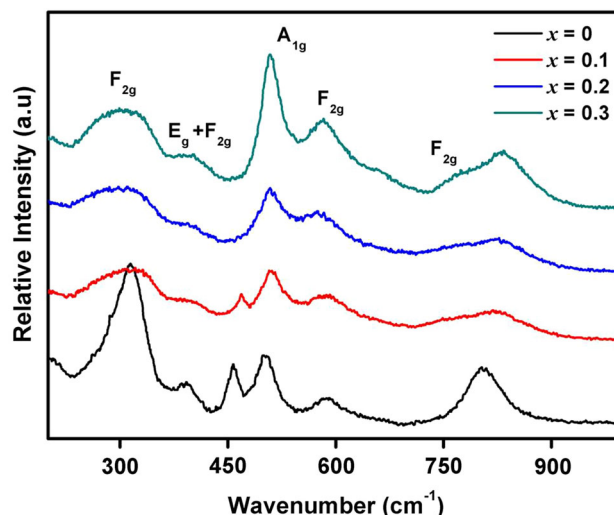

Fig. 2 FT Raman spectra of $(CaCe_{1-2x}Mn_{2x})(Sn_{1-x}Mn_xNb)O_{7-\delta}$ ($x = 0, 0.1, 0.2$ and 0.3) samples sintered at 1,250 °C for 9 h

reported by Vandenborre et al. that the Sn^{4+} ions will develop a strong force field in the octahedral network due to its high electronegativity (~ 1.96) and this makes the stannate pyrochlores more rigid and stable structures than their titanate, zirconate or niobate counterparts [15]. In the present investigation, by substituting less electronegative Mn (~ 1.55) ions in the Sn site, the force constant of B–O bond decreases due to the decreased covalent nature and hence the force field of the whole crystal decreases with the progressive Mn substitution. This will induce some distortions in the BO_6 octahedral network leading to local disordering of the structure. These variations are reflected as the increased intensities of the A_{1g} and F_{2g} modes related to B–O vibrations. This is further evidenced by the increased intensity of the mode appearing ~ 830 cm^{-1} which is reported in the literature as a combination band arises due to the distortion of BO_6 octahedra and subsequent relaxation of the selection rules [16]. Hence Raman spectroscopy has been used here as a probe to local disordering in the structure which are not observable in X-ray diffraction studies.

3.3 Scanning electron microscopy studies

SEM micrographs of the sintered samples are shown in Fig. 3. Micrographs show well dense grains with high density for Mn substituted compounds. An increase in relative density can be observed from 82 to 97 % with increase in Mn substitution (Table 1). The grain size of the sintered microstructure was calculated by linear intercept method and the values are listed in Table 1. The average grain size increases with substitution up to $x = 0.2$ and thereafter a decreasing trend can be observed. Also, the
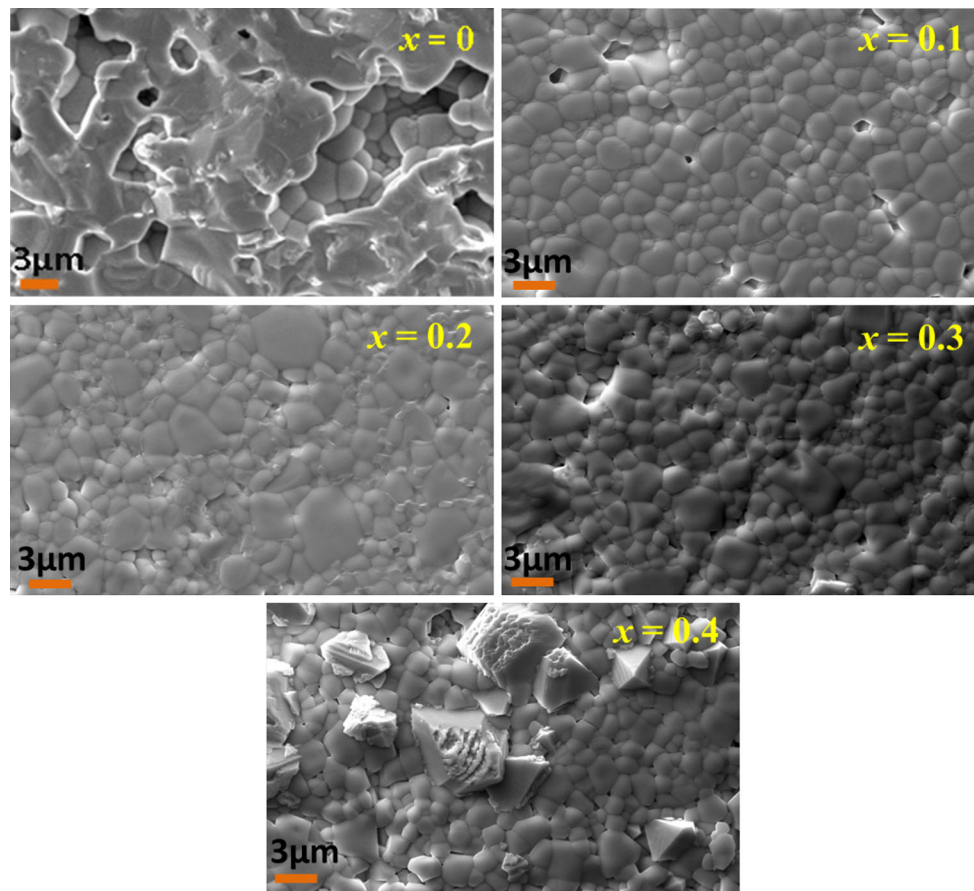
Fig. 3 SEM images of $(CaCe_{1-2x}Mn_{2x})(Sn_{1-x}Mn_xNb)O_{7-\delta}$ ($x = 0, 0.1, 0.2, 0.3$ and 0.4) samples sintered at 1,250 °C for 9 h

Table 1 Relative density, average grain size and equivalent circuit fitting parameters of $(CaCe_{1-2x}Mn_{2x})(Sn_{1-x}Mn_xNb)O_{7-\delta}$ (x = 0, 0.1, 0.2 and 0.3) samples

Composition $(CaCe_{1-2x}Mn_{2x})$ $(Sn_{1-x}Mn_xNb)O_{7-\delta}$	Relative density (%)	Average grain size (μm)	Equivalent circuit fitting parameters					
			Q_g (pF)	n_g	R_g (kΩ)	Q_{gb} (pF)	n_{gb}	R_{gb} (kΩ)
$x = 0$	82							
$x = 0.1$	94	1.47 ± 0.54	16	0.87	306	–	–	–
$x = 0.2$	96	2.14 ± 0.72	61	0.89	122	–	–	–
$x = 0.3$	97	1.3 ± 0.46	22	0.9	2,100	70	0.91	66,000

presence of secondary phases can be clearly seen in the micrograph for $x = 0.4$.

3.4 Impedance analysis

Complex impedance spectroscopy is widely used to analyze the electrical behavior of the system. Cole–Cole plot analysis provides to study the various contributions from grain, grain boundary and electrode effect on the relaxation processes involved in the polycrystalline materials [17]. Figure 4 shows the Cole–Cole plots of $(CaCe_{1-2x}Mn_{2x})$ $(Sn_{1-x}Mn_xNb)O_{7-\delta}$ ($x = 0, 0.1, 0.2, 0.3$ and 0.4) at 300 °C. The graph is characterized by only one semicircle.

The value of resistance can be determined from the intercepts of the semicircle on the real axis Z′. The value of resistance decreases with Mn substitution for the compositions up to $x = 0.2$ and then an abrupt increase can be observed for $x = 0.3$. Increased carrier concentration with Mn substitution may be one of the reasons for the decreased resistance which is discussed in the later part of text. To some extent, the microstructural variation in the samples with progressive substitution may be the reason for this behavior. Slightly increased grain size can be observed for the samples up to $x = 0.2$ and which may drive to a decrease in resistance. The sudden decrease in grain size, i.e., an increased grain boundary contribution which acts as
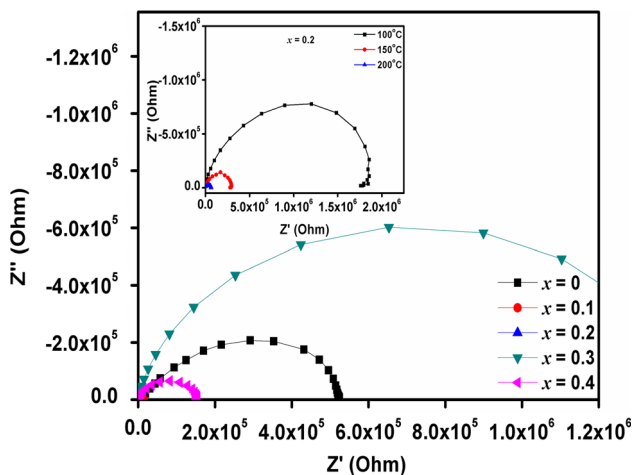
Fig. 4 Cole−Cole plots of $(CaCe_{1-2x}Mn_{2x})(Sn_{1-x}Mn_xNb)O_{7-\delta}$ ($x = 0$, 0.1, 0.2, 0.3 and 0.4) samples at 300 °C. *Inset of the figure shows the Cole–Cole plot for the composition $x = 0.2$ at different temperatures*

Fig. 5 a Cole–Cole plot of experimental and simulated fit and its equivalent circuit for the composition $x = 0.3$ at 150 °C and **b** modulus spectra for $x = 0.3$ at different temperatures

a blocking barrier for conduction may be a reason for the increased resistance of these samples. The inset of the figure shows the Cole–Cole plot for $x = 0.2$ at different temperatures. It can be seen that the value of resistance decreases with temperature, indicates the NTCR behavior of the material. All other samples show the same type of behavior.

Impedance data could often be modeled by an equivalent circuit that provides a realistic representation of the electrical properties. The equivalent circuit consists of a series of three parallel RC networks for the grain, grain boundary and ceramic–electrode interfaces. However, for semicircles with a center below the X-axis, an accurate fit is obtained usually by substituting the ideal capacitor by a constant phase element (CPE). The impedance of CPE is: $Z_{CPE} = 1/Q(j\omega)^n$, where Q indicates the value of capacitance of the CPE element and n is the fractal exponent, represents the deviation from ideal capacitor behavior. The value of n is unity for a pure capacitor and is zero for a pure resistor. Figure 5a shows the best fit between the observed and calculated values for $x = 0.3$ at 150 °C using the software ZSimpwin. The electrical properties are represented by two parallel R-CPE circuits connected in series which is the accepted representation for a polycrystalline material containing grain and grain boundary. The nonhomogeneity associated with the microstructure of the material may lead to the introduction of the CPE elements. High frequency arc is associated with grain and the low frequency arc with grain boundaries. The fitted parameters are shown in Table 1. The given range of n values represents the interaction between localized sites in Mn substituted samples. The capacitance values are similar to the earlier reported Mn containing compounds [18].
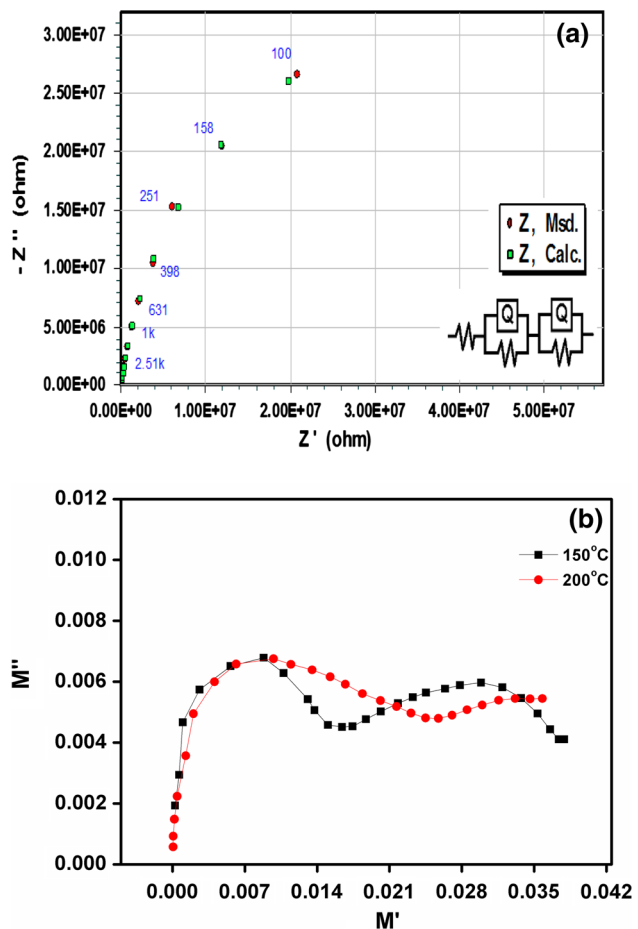
Electric modulus can be effectively used to analyse the capacitance values in equivalent circuit since the modulus spectra is dominated by the RC element with smaller capacitance. Figure 5b shows the modulus spectra for $x = 0.3$ at 150 and 200 °C. The presence of two semicircles in the spectra confirms the contribution of both grain and grain boundary. The grain contribution moves out of the frequency domain rapidly as the temperature increases and for temperatures ≥ 200 °C the spectra is dominated by the grain boundary. The peak maximum frequency for each R-CPE element is given by

$$\omega_{max}(RQ)^{1/n} = 1 \qquad (2)$$

where R and Q are the resistance and CPE values of the material at a particular temperature T. The grain boundary resistance found to decrease with increase in temperature. Capacitance values for grain and grain boundary contributions calculated from this expression are 20 and 69 pF respectively and are close to the values obtained from the Cole–Cole plot.
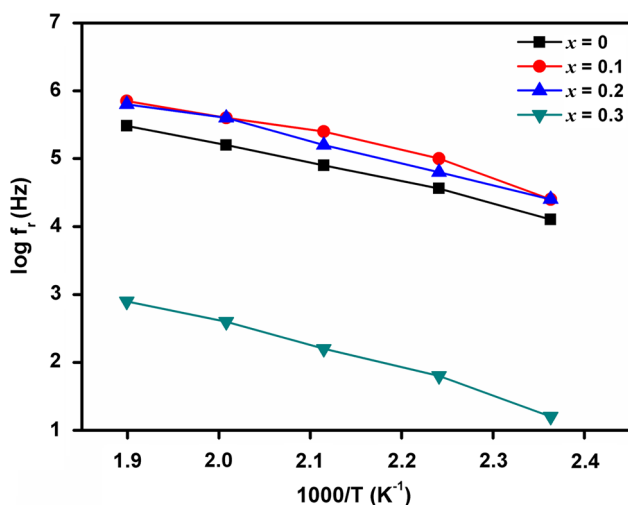
Fig. 6 Variation of relaxation frequency of $(CaCe_{1-2x}Mn_{2x})(Sn_{1-x}Mn_xNb)O_{7-\delta}$ ($x = 0, 0.1, 0.2$ and 0.3) samples with temperature

Fig. 7 Arrhenius plots of $(CaCe_{1-2x}Mn_{2x})(Sn_{1-x}Mn_xNb)O_{7-\delta}$ ($x = 0, 0.1, 0.2, 0.3$ and 0.4) samples

Under ac electric field, motion of the charge carriers will cause a temperature dependent relaxation [19] and the relaxation frequency will be a measure of the cause of conduction (either grain or grain boundary property) present in the material. Figure 6 shows the variation of relaxation frequency with temperature for different Mn concentration. For all the compounds an increase in relaxation frequency can be observed with temperature. This is a clear indication of hopping type conduction in the given materials [19]. Further, the relaxation frequency of compounds in the range $0 \leq x \leq 0.2$ falls in the high frequency region while compounds with higher Mn concentration fall in the low frequency region. In impedance spectra, the bulk properties or grain effects are exhibited at high frequencies and the grain boundary effects at low frequencies. Hence it can be concluded that the compositions in the range $0 \leq x \leq 0.2$ exhibit the grain effects and the $x = 0.3$ and 0.4 display the grain boundary dependent properties.

3.5 Electrical conductivity studies

Figure 7 depicts the variation of dc conductivity of the system with temperature. All the compounds show the NTCR behavior as the conductivity increases with increase in temperature. Our previous studies showed that Mn will stabilize at the A-site of the pyrochlore as Mn^{2+}. The electrons released during the reduction of Ce^{4+} and Mn^{4+} to Ce^{3+} and Mn^{2+} by the removal of excess oxygen in the lattice make the compounds semiconducting. Consequently, the charge carrier concentration increases with Mn substitution. Since Ce and Mn can exist in different oxidation states, these defect states can act as channels for
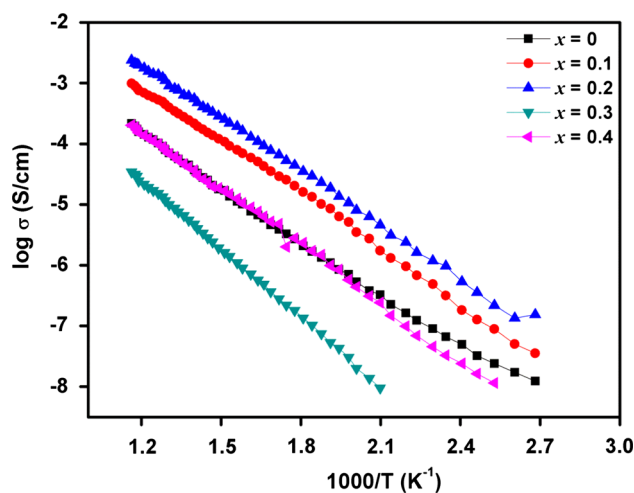
hopping type conduction of electrons in the given temperature range. The conductivity was found to increase with Mn substitution up to $x \leq 0.2$ and decreased for higher concentrations. Increase in charge carriers and grain size with substitution may be the reason for the increase in conductivity. For higher Mn concentration, the grain boundary effect is the dominant factor deciding the properties as evidenced by the microstructure and impedance analysis. Also a decrease in grain size can be observed from the microstructure. Electrons associated with Mn^{2+} are strongly localized and together with the decreased grain size may produce electrical barriers at the grain boundaries and can decrease the electron mobility. This may be the reason for the appearance of grain boundary dependent conductivity for higher Mn concentrations as confirmed from the impedance analysis. Electrical conductivity of all the given materials is a thermally activated process and follows the Arrhenius law given by

$$\sigma_{dc} = \sigma_o \exp(-Ea/kT) \tag{3}$$

where σ_o is the pre-exponential factor, Ea is the activation energy and k is the Boltzmann constant. Activation energy calculated from the slope of the Arrhenius plots are given in Table 2. Activation energy was found to increase slightly with Mn concentration due to the strongly localized electrons associated with Mn^{2+} ions. More number of electrons gets localized and requires more energy to hop from one site to another as the Mn concentration increases. The activation energy values suggest similar type of hopping conduction mechanism exists in the given materials. The relation between resistance and temperature for a negative temperature coefficient thermistor is expressed by the following equation:

Table 2 Activation energy and thermistor parameters of $(CaCe_{1-2x}Mn_{2x})(Sn_{1-x}Mn_xNb)O_{7-\delta}$ ($x = 0, 0.1, 0.2, 0.3$ and 0.4) samples

Composition $(CaCe_{1-2x}Mn_{2x})$ $(Sn_{1-x}Mn_xNb)O_{7-\delta}$	Activation energy (eV)	Thermistor constant $\beta_{300/600}$ (K)	Sensitivity α (K^{-1})		Aging constant at 600 °C (%)
			300 °C	600 °C	
$x = 0$	0.55	6,706	−0.0204	−0.0088	2.17
$x = 0.1$	0.57	6,750	−0.0205	−0.0088	1.05
$x = 0.2$	0.58	7,500	−0.0228	−0.00984	0.91
$x = 0.3$	0.71	8,410	−0.0256	−0.0110	0.83
$x = 0.4$	0.62	7,700	−0.0234	−0.0101	1.4

$$R_T = R_N \exp[\beta(1/T - 1/T_N)] \quad (4)$$

where R_T is the resistance at temperature T, R_N is the resistance at temperature T_N known, and β is a thermistor constant. From the above relation the thermistor constant can be calculated using the following equation:

$$\beta = [TT_N/(T_N - T)]\ln(R_T/R_N) \quad (5)$$

The sensitivity of a thermistor is defined by the temperature coefficient of resistance α. The sensitivity can be expressed as a function of thermistor constant by the relation;

$$\alpha = 1/T(dR/dT) = -\beta/T^2 \quad (6)$$

The thermistor parameters of the system calculated using the above equations is given in the Table 2. Thermistor constant (β) is calculated in the temperature range from 300 to 600 °C. β was found to be enhanced for higher Mn concentrations. Thermistor constant of the system lies in the range 6,700–8,500 K and the sensitivity values are in the range −1 to −2 %. The aging tests at 600 °C on the given samples reveal that the variation of aging constant (dR/R) is 0.8–2 % for the time period of 500 h. Highly dense Mn substituted compounds are found to be more resistant to aging. All the compositions show better thermistor properties compared with many of the spinel and pyrochlore based systems [8, 9]. From the results it is clear that the thermistor properties can be tuned to desired values by the double substitution of Mn on both A and B site of the pyrochlore. By incorporating more Mn^{2+} in the A site of the pyrochlore by double substitution, we were able to improve the thermistor properties due to the increased localization effect of electrons as compared with our previous studies.

4 Conclusions

Dependence of electrical properties on structure and microstructure of $(CaCe_{1-2x}Mn_{2x})(Sn_{1-x}Mn_xNb)O_{7-\delta}$ ($x = 0, 0.1, 0.2, 0.3$ and 0.4) pyrochlore type oxides through the simultaneous substitution of Mn in both A and B site has been investigated. X-ray diffraction and Raman spectroscopy studies confirm the cubic pyrochlore structure of the compounds. Electrical conductivity was found to be increased with Mn concentration particularly for compounds showing grain/bulk electrical properties while it showed a decreasing trend in the grain boundary dominant compounds. All the compounds exhibited good NTC thermistor properties which are tunable with Mn double substitution and may find application in high temperature thermistors.

References

1. Z. Hiroi, J.-I. Yamaura, S. Yonezawa, H. Harima, Phys. C: Supercond. **460**, 20 (2007)
2. M. Deepa, P. Prabhakar Rao, A.N. Radhakrishnan, M.R. Chandran, P. Koshy, Mater. Chem. Phys. **127**, 162 (2011)
3. M.A. Subramanian, A.P. Ramirez, G.H. Kwei, Solid State Ion **108**, 185 (1998)
4. A. Zhang, M. LU, Z. Yang, G. Zhou, Y. Zhou, Solid State Sci. **10**, 74 (2008)
5. S. Sumi, P. Prabhakar Rao, S.K. Mahesh, P. Koshy, Mater. Res. Bull. **47**, 4365 (2012)
6. P. Garcia Casado, J.A. Alonso, J.L. Martinez, M.T. Fernandez, I. Rasines, Chem. Mater. **12**, 1217 (2000)
7. S. Brahma, R.N.P. Choudhary, A.K. Thakur, Phys. B: Condens. Matter. **355**, 188 (2005)
8. A. Feteira, J. Am. Ceram. Soc. **92**, 967 (2009)
9. M.A.L. Nobre, S. Lanfredi, Appl. Phys. Lett. **82**, 2284 (2003)
10. E.J. Verwey, P.W. Haayman, F.C. Romeijn, J. Chem. Phys. **15**, 181 (1947)
11. R.A. McCauley, J. Appl. Phys. **51**, 290 (1980)
12. D.L. Rousseau, R.P. Bauman, S.P.S. Porto, J. Raman Spectrosc. **10**, 253 (1981)
13. B.P. Mandal, P.S.R. Krishna, A.K. Tyagi, J. Solid State Chem. **183**, 41 (2010)
14. I. Kosacki, T. Suzuki, H.U. Anderson, P. Colomban, Solid State Ion **149**, 99 (2002)
15. M.T. Vandenborre, E. Husson, J. Solid State Chem. **50**, 362 (1983)
16. A.N. Radhakrishnan, P. Prabhakar Rao, S.K. Mahesh, D.S. Vaisakhan Thampi, P. Koshy, Inorg. Chem. **51**, 2409 (2012)
17. K.S. Cole, R.H. Cole, J. Chem. Phys. **9**, 341 (1941)
18. M.J. Tung, T.Y. Tseng, M.J. Tsay, W.C. Chang, J. Phys. IV Fr **07**, C1–C129 (1997)
19. M.M. Hassan, J. Phys. D Appl. Phys. **43**, 155401 (2010)